ELSEVIER

Materials Science and Engineering A xxx (2004) xxx–xxx

MATERIALS SCIENCE & ENGINEERING A

www.elsevier.com/locate/msea

Impression creep characterization of rapidly cooled Sn–3.5Ag solders

I. Dutta*, C. Park, S. Choi

Department of Mechanical Engineering, Center for Materials Science and Engineering, Naval Postgraduate School, Monterey, CA 93943, USA

Received 13 August 2003; received in revised form 3 March 2004

Abstract

The creep behavior of solders crucially influences solder joint reliability in microelectronic packages. This, in conjunction with the ongoing industry-wide transition to lead-free solders, has resulted in significant current emphasis on developing approaches for expeditiously creep testing miniaturized samples of a wide range of solder compositions to determine their suitability for packaging applications. Here we characterize the creep response of Sn–3.5Ag solders via impression creep testing. The tested microstructures represent a rapidly cooled state, resembling the highly refined microstructures often found in tiny microelectronic solder joints. It is shown that in the as-reflowed state, the solder creeps by a viscous glide-controlled mechanism at low stresses due to the presence of a non-equilibrium amount of dissolved Ag in Sn, and a particle-limited climb mechanism at high stresses. Following slight aging, which allows the dissolved solute concentration to drop to near-equilibrium levels, the low stress mechanism changes to dislocation climb-control. Based on these observations, a unified view of creep of Sn–3.5Ag solders is presented, which is consistent with observations of a transition from low to high stress sensitivity with increasing stress, which has been reported in several studies.

Keywords: Impression creep; Sn–Ag; Lead-free solder; Mechanism

1. Introduction

During service, microelectronic solder joints are exposed to aggressive thermo-mechanical cycling (TMC), with imposed shear strains and homologous temperatures (T_m) frequently approaching 30% and 0.9, respectively. Consequently, the joint undergoes extensive creep, resulting in the accrual of large inelastic strains with progressive cycling, which in turn often leads to failure via low-cycle fatigue [1]. The creep properties of solders are therefore crucial for accurate performance and reliability predictions of microelectronic solders. As the microelectronics industry adopts new generations of environmentally friendly lead-free solders in response to worldwide legislation, there is a particular need to develop comprehensive creep databases of these alloys. Therefore, there is significant current interest in characterizing the creep behavior of emerging lead-free solders, among which the eutectic 96.5%Sn–3.5%Ag is one of the most promising. In this article, we report on data obtained on Sn–Ag solder via impression creep testing.

The technique of impression creep wherein a flat-tipped cylindrical indenter is used to load the sample in nominal compression, allows steady state to be established within a relatively short time [2–6]. The approach requires minimal sample preparation, allows multiple creep curves to be generated from different locations within the same sample, and can reliably replicate uniaxial creep data produced on bulk samples [2,3,7]. Furthermore, because of its ability to probe small material volumes, the technique is scaleable for testing of small microelectronic joints, which may behave quite differently from the bulk alloy [8].

Although a number of studies on creep of Sn–Ag solders have been reported [9–15], there exist significant discrepancies in the available data, as shown in Table 1. In general, all the data can be divided into two stress regimes, with the stress exponent n ranging from 4 to 7 in the low stress regime, and from 7 to 12 in the high stress regime. In most cases, the activation energy Q has been thought to be associated with dislocation core diffusion, although in some cases, it falls well below the range of 40–65 kJ/mole for core diffusion in pure Sn (see Table 1). Some of these discrepancies may be attributed to solidification rate dependent microstructural differences in the experimental samples due to differences in sample size (bulk versus small joints).

* Corresponding author. Tel.: +1-831-656-2851; fax: +1-831-656-2238.
E-mail address: idutta@nps.navy.mil (I. Dutta).

0921-5093/$ – see front matter © 2004 Published by Elsevier B.V.
doi:10.1016/j.msea.2004.03.023

Table 1
Summary of available creep data on Sn–Ag solder (references [9–15])

Q (kJ/mole)	n	T/T_m range	σ/G range ($\times 10^4$)	$Q_{reference}$ for Sn
39 [9]	5.5 [9]	0.6–0.80	3–30	
51 [11], 66 [12]	10 [11], 5 [12]	0.6–0.92	1–5	Q_{vol} = 108 kJ/mole
25 [10]	12 [10]	0.6–0.87	8–40	[16]
80 [13]	4–5, 7–11 [13]	0.66–0.81	2–20	Q_{gb} = 70 kJ/mole
–	11 [14]	0.76	4–12	[16]
80–97 [15]	7 [15]	0.6–0.8	3–27	Q_{core} =40–64 kJ/mole [15,17–19]

Indeed, the creep rate of Sn–Ag solders has been found to depend quite significantly on the cooling rate following reflow [14,20]. Furthermore, bulk solder samples usually display considerable spatial (i.e. volumetric) variations in the microstructure due to differences in local solidification rate [21], potentially influencing the resultant data.

Although obtained on bulk samples, the impression creep data reported here, by probing small volumes of material on a single sample plane with constant microstructure, avoids many of the above pitfalls. It will be demonstrated that despite some apparent anomalies, the data obtained here are fully consistent with a combination of conventional creep mechanisms with reasonable values of n and Q.

2. Experimental procedure

2.1. Sample preparation

Ingots of eutectic 96.5%Sn–3.5%Ag were obtained from Alpha Metals, Jersey City, New Jersey, USA. Small pieces of this ingot were cut off and reflowed at 553 K in a cylindrical Al mold of 25 mm diameter, 10 mm height and 1 mm wall thickness. After reflow, the mold, with the solder in it, was quenched in water. In order to prevent the molten solder from splattering, a two-step quench was used. The bottom of the mold, which consisted of an Al sheet about 0.25 mm in thickness, was first brought briefly in contact with water till a solid skin formed on the free surface (~2 s), followed by complete immersion in the quenching medium. This procedure, which resulted in a cooling rate of ~31 K/s between 553 and 463 K, and ~20 K/s between 463 and 333 K at the bottom surface of the sample, produced a highly refined microstructure resembling microstructures often found in tiny flip-chip (FC) and ball-grid array (BGA) microelectronic solder joints[1]. Subsequently, the sample was extracted from the mold, and the bottom surface was ground and polished to a 1 μm finish in preparation for impression creep testing. Fig. 1a shows the microstructure of the bottom surface in the as-reflowed state, revealing secondary dendrite arms of primary β-Sn, with intervening regions of a highly refined eutectic microconstituent. Fig. 1b shows a magnified scanning electron micrograph (using secondary electrons), revealing that the divorced eutectic microconstituent between primary Sn regions comprises a uniform dispersion of very fine (~0.3–0.5 μm) Ag_3Sn particles in a β-Sn matrix. After sample preparation, the solder specimens were stored at

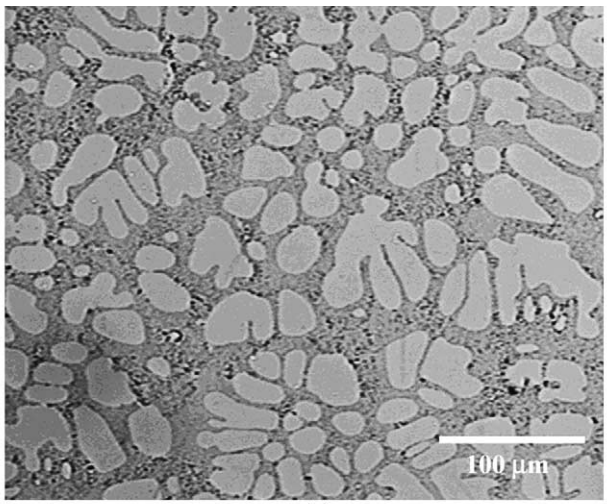

Fig. 1. (a) Optical micrograph of the test sample showing secondary dendrites of primary β-Sn, with intervening regions of eutectic. (b) Secondary electron image showing that the eutectic comprises of a dispersion of very fine (0.3–0.5 μm) Ag_3Sn particles in a β-Sn matrix.

[1] Although the nominal cooling rate of microelectronic packages in the reflow furnace is typically around 3–5 K/s, local cooling rates of the tiny solder balls in the package can be substantially greater, necessitating the use of high cooling rates on bulk samples in order to reproduce microstructures found in small joints.

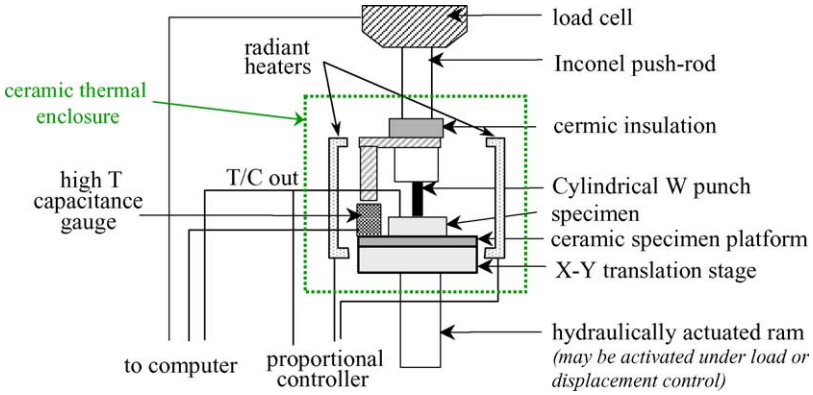

Fig. 2. Schematic of the experimental apparatus for impression creep testing.

273 K in order to prevent natural aging of the microstructure until they were ready to be tested.

2.2. Impression creep testing

The test sample was placed on a self-leveling specimen platform, which was mounted on an *X–Y* translation stage so that multiple tests could be run on the sample without removing it from the self-leveling arrangement. A 1 mm diameter flat-tipped cylindrical tungsten punch, connected to a servo-hydraulic MTS frame equipped with an appropriate load cell was utilized to apply a constant load, which produced a nominally constant compressive punch stress σ_p on the sample. The resulting time-dependent punch displacement δ (i.e. the impression depth) was measured with a capacitance displacement gauge attached to the punch chuck. Dual radiant heaters interfaced by a proportional controller were used to heat both the sample and the punch simultaneously during testing. The instrumentation allowed load, displacement and temperature stabilities of ± 0.05 N, ± 0.06 μm and $\pm 0.1\,^{\circ}$C, respectively. A schematic of the apparatus is shown in Fig. 2. The creep tests covered a σ_p[2] and T ranges of 12–50 MPa and 323–423 K, respectively, resulting in a σ_p/G range of 5×10^{-4} to 5×10^{-3}, and T/T_m range of 0.65–0.86, where the shear modulus G is given by G (MPa) $= 19406.67 - 28.2T\,^{\circ}$C [9].

Even though the specimen stage was self-leveling (via a universal ball-joint mount), it was found that maintaining perpendicularity between the punch axis and the specimen surface was very difficult. This was evidenced by punch impressions which were frequently gibbous even after prolonged testing. This resulted in an exaggerated primary stage, making the establishment of a true steady state difficult in reasonable time. In order to circumvent this problem, the following test methodology was adopted. The specimen was first indented using a punch stress of 50 MPa in order to ensure complete contact between the punch tip and the sample. Then, the applied stress was reduced to 1 MPa, and held constant at the test temperature for 5–8 h in order to allow the plastic zone under the punch to recover partially. Subsequently, the applied stress was increased to the test stress and held constant to produce the creep curve. In addition to establishing complete contact between the punch and sample, this procedure, by creating a fully developed plastic zone under the punch prior to the creep test, allows the Von–Mises effective stress distribution under the punch to be rapidly stabilized, substantially shortening the time required to achieve a steady-state impression velocity [23].

For power law creep behavior, the steady state impression velocity is given by

$$V = A' f(\phi) \left(\frac{Gb}{kT}\right) \left(\frac{\sigma_p}{G}\right)^n e^{-Q/RT} \quad (1)$$

where $\sigma_p \approx 3.5\times$ the equivalent uniaxial stress (σ), the constant A' incorporates the Dorn constant A, as well as a factor to convert σ to σ_p, and $f(\phi)$ is a function of the punch diameter ϕ, such that $\dot{\delta}/f(\phi)$ is the average creep strain rate in the plastic zone under the punch. It has been shown that the parameter $f(\phi)$, representing the depth of the plastic zone under the indenter, stays approximately constant and equal to ϕ during steady state creep [22]. Thus, since A', $f(\phi)$, b and k are constants.

$$\frac{VT}{G} \propto \left(\frac{\sigma_p}{G}\right)^n e^{-Q/RT} \quad (2)$$

this allows us to obtain the activation energy Q from a plot of $\ln[VT/G]$ versus $1/T$ at constant σ_p/G, and the stress exponent n from a plot of $\ln[VT/G]$ versus σ_p/G at constant T.

3. Results and discussion

Fig. 3 shows examples of impression creep plots for the as-reflowed solder at various stresses and temperatures. Clearly, complete creep curves are obtainable via this technique in a relatively short time, with a steady state impression velocity V being established within about 4–5 h for most test conditions. Fig. 4 shows a plot of the quantity

[2] The punch stress σ_p is about 3–3.5 times the equivalent uniaxial compressive stress, depending on the specific material properties [22,23].

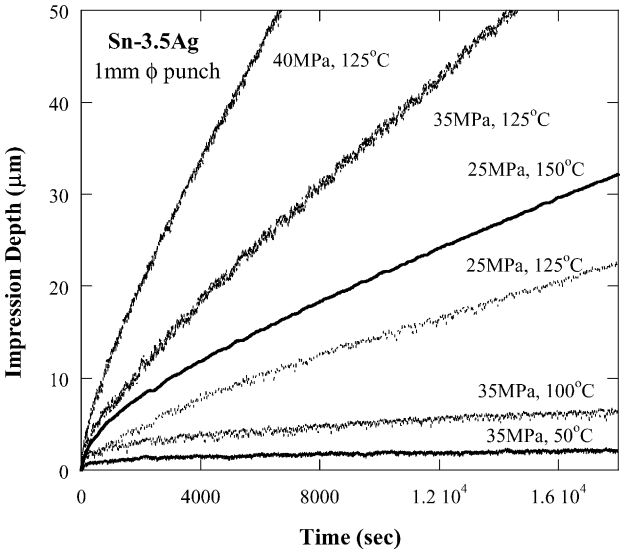

Fig. 3. Typical impression creep plots for Sn–3.5Ag solder at various stresses and temperatures.

$V(T/G)$ versus modulus compensated punching stress (σ_p/G) at various temperatures. The plots for 323, 373 and 398 K naturally divide into low and high stress regimes, exhibiting a clear mechanism transition from power-law with $n \approx 3$ in the low stress regime, and a greater stress dependence at higher stresses. The apparent stress exponent (n_{app}) in the high stress regime is ~9. At 423 K, the plot shows a greater slope, corresponding to $n \approx 4.4$. The reason for the different behavior at 423 K will be discussed later.

The observed mechanism transition from low to high stresses at 323–398 K is consistent with observations of two distinct regimes of creep in both pure Sn and Sn-based solders [13]. However, our n value of 3 is lower than those obtained by other investigators (typically, $n \sim 4$–5 [9,13,24]). This is attributable to the different starting microstructure, as dictated by the cooling rate, and will be discussed below. Although, in consistence with our observations, creep in the high stress regime has been previously described as being governed by power-law with a high stress exponent ~8–11 [10,11,13–15,20], a mechanism to explain this transition to a high n-value has been elusive. This issue is addressed in further detail subsequently.

Fig. 5 shows plots of $\ln[V(T/G)]$ versus $1/T$ at constant σ_p/G values in both the low and high stress regimes. In the low stress regime ($\sigma_p/G < 2 \times 10^{-3}$), the activation energy Q is 43–46 kJ/mole. This value is in agreement with Q values of 46 kJ/mole obtained via impression creep of single crystal β-Sn [24], and compares reasonably well with Q of ~40 kJ/mole obtained via testing of Sn–3.5Ag solder bumps in a double lap-shear geometry [9]. However, our Q value is considerably smaller than other reported values of 60–85 kJ/mole in the low stress regime [12,13], suggesting that a different mechanism is operative. In the high stress

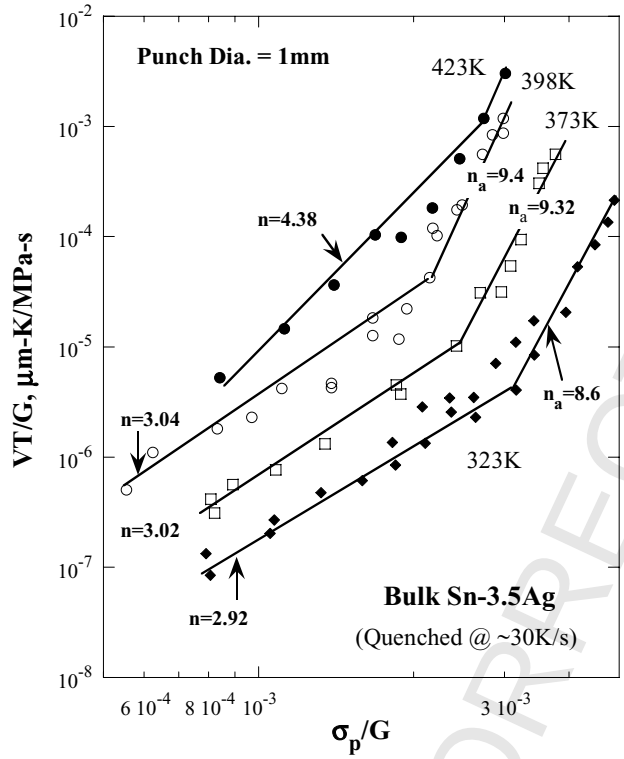

Fig. 4. Punch stress dependence of impression velocity. The data naturally divide into high and low stress regimes, with $n \approx 3$ for 323–398 K in the low stress regime, and $n_{app} \sim 9$ in the high stress regime. At 423 K, a greater stress dependence ($n \approx 4.4$) is observed in the low stress regime.

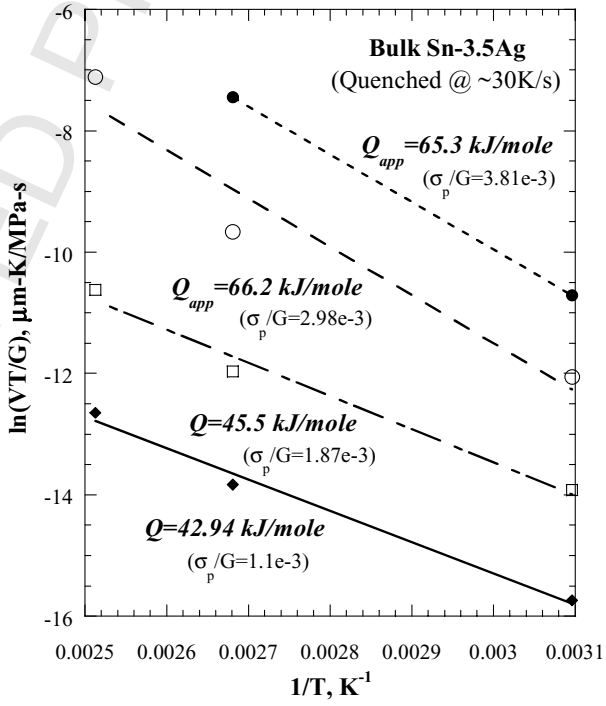

Fig. 5. Temperature dependence of impression velocity, showing that in the low stress regime (where $n \sim 3$), the activation energy Q ranges from 43 to 46 kJ/mole. In the high stress regime, the apparent activation energy $Q_{app} \approx 66$ kJ/mole.

regime ($\sigma_p/G \geq 2.8 \times 10^{-3}$), the apparent activation energy is 65–66 kJ/mole, and is nominally consistent with the acitvation energy of core diffusion in Sn [15].

Although there is significant discrepancy in the reported activation energy data for Sn and Sn-based solders because of the high degree of anisotropy in tetragonal Sn, and Q values of 40–60 kJ/mole are often associated with dislocation pipe diffusion in Sn [9,17,18,24], the n value of 3 obtained here in the low stress regime is inconsistent with a dislocation pipe diffusion assisted climb-controlled creep mechanism. However, our Q value of ~45 kJ/mole is nominally consistent with the value of 50 kJ/mole reported for diffusion of Ag in Sn [16]. This, in conjunction with $n \approx 3$, strongly suggests that for the rapidly cooled microstructures of this study (~30 K/s), viscous glide of dislocations, limited by solute-drag, is the rate controlling mechanism. The rapid cooling rate enables a non-equilibrium amount of Ag atoms to be retained in solution in Sn, allowing the solute to interfere with slip, which becomes slower than climb, thus becoming rate-controlling (class A, i.e. alloy, behavior).[3]

The condition for transition from climb-controlled class M (pure metal) to glide-controlled class A behavior may be expressed as [26,27]:

$$\left(\frac{\sigma}{G}\right)^2 \geq \frac{1}{\varsigma}\left[\frac{kT}{eGb^3}\right]^2\left(\frac{1}{c}\right)\left(\frac{Gb}{\gamma}\right)^3\left(\frac{\tilde{D}}{D_v}\right) \quad (3)$$

where c is the solute (Ag) concentration in the β-Sn matrix, $\tilde{D}$ the Ag diffusivity in Sn, D_v the volume self-diffusivity in Sn, γ the stacking fault energy of Sn, ς the constant with a value on the order of 10^{12} for most metals, k the Boltzmann constant, b the Burger's vector, and e the solute–solvent size difference [26]. The value of e can be estimated to be ~0.086 from the free atomic radii of Sn and Ag (1.4 and 1.52 Å, respectively [28]). Although there are two prominent Burger's vectors in Sn, the most active slip system appears to be $(1\,1\,0)1/2\langle 1\,1\,1\rangle$ [24,29,30], yielding $b = 4.418$ Å. The data for the stacking fault energy of Sn is not readily available, but it is thought to be relatively high since transmission electron microscopy does not reveal widely spaced partials [29]. Hence, we estimate γ to be ~100 J/m^2. The volume self-diffusivity of Sn is given by $D_v \approx (12.8 \times 10^{-4})\exp(-109{,}000/RT)$ m^2/s [16,31], whereas the inter-diffusivity of Ag in Sn may be expressed as $\tilde{D} \approx (7.1 \times 10^{-7})\exp(-51{,}500/RT)$ m^2/s [16], producing $\tilde{D}/D_v \approx 4.6 \times 10^8$ at 373 K. Since the solubility limit of Ag in Sn is ~0.09% at the eutectic temperature (494 K) [32], we assume that at the creep test temperatures, $c \approx 0.0005$ (i.e. 0.05%). However, if the Sn–3.5%Ag alloy is rapidly cooled after reflow (e.g. at ~30 K/s, as in this study), it is likely that as much as 1 at.% of the Ag may be retained in solution in Sn within the interdendritic eutectic regions (see Fig. 1a). Inserting these values into Eq. (3), we find that at 373 K, the transition from climb-control to viscous glide will occur at $\sigma_p/G \approx 3 \times 10^{-3}$ for $c = 0.0005$, but at $\sigma_p/G \approx 5 \times 10^{-4}$ for $c = 0.01$.[4] Comparing these results with Fig. 4, it is observed that the $n = 3$ region at 373 K extends down to $\sigma_p/G \sim 8 \times 10^{-4}$, which is above the predicted start of glide-control at $\sigma_p/G \approx 5 \times 10^{-4}$ at this temperature. This was also found to be true for the other temperatures, where, the assumption of 1%Ag in solution satisfied the condition for viscous glide (i.e. Eq. (3)) over the low stress regime for all the plots in Fig. 4. Thus the calculation above shows that in Sn–3.5Ag, viscous drag can operate if a sufficient amount of solute is retained in solution during quenching. However, when an equilibrium amount of solute is present in solution, the transition to viscous drag can theoretically occur only at high σ_p/G values (e.g. 3×10^{-3} for $c = 0.0005$ at 373 K), where, as seen in Fig. 4, it is masked by a faster mechanism. Clearly, for Sn–Ag alloys which contain an equilibrium amount of solute, or which are only slightly supersaturated, viscous drag cannot occur, and the low stress regime is dominated by a climb-controlled mechanism with $n \sim 4$–5 (e.g. [9,12,13]).The plot at 423 K shows a different behavior from that observed at 323–398 K. These tests were conducted on a sample which had already been subjected to over 200 h of testing at 398 K and several hours at 423 K. This inadvertent aging allowed Ag to precipitate out of the supersaturated Sn in the form of additional Ag_3Sn particles, thereby reducing c, and causing the creep mechanism to transition to climb-control with $n \approx 4.4$. Despite this transition from glide at $T \leq 398$ K to climb-control at 423 K, it is observed that the creep rate at 423 K is not as high relative to 398 K as would be expected. This is probably because the increased amount of Ag_3Sn dispersion slows the rate of climb-controlled creep in proportion to the particle size and volume fraction [34,35].

At high stress levels, the creep rate displays a substantially greater stress dependence than those indicated by glide or climb control. There are three possible mechanisms which may explain this. These are: (1) the start of power-law breakdown (PLB); (2) breakaway of gliding dislocations from solute atmosphere, leading to a transition from glide-control to climb control; and (3) transition to particle-limited climb with a high n.

Creep via PLB typically occurs at diffusivity normalized strain rate ($\dot{\varepsilon}/D_v$) values of $>10^{13}$ m^{-2} [38]. Inspecting the present data (e.g. at 373 K), we observe that the high stress regime (with enhanced stress sensitivity) begins around 5×10^{11} m^{-2} at 373 K. This is nearly one and a half orders of magnitude below the $\dot{\varepsilon}/D_v$ value at which PLB creep is

[3] The retention of a non-equilibirum amount of Ag in Sn following quenching has been evidenced by an increase in ambient temperature flow stress following aging (1–3 days at 453 K), which is attributable to increased precipitation of Ag_3Sn as the excess Ag comes out of solution [W.D. Armstrong, University of Wyoming, Private Communication].

[4] Here we use $\sigma_p \approx 3.5\sigma$ to convert the stress in Eq. (3) into punch stress.

expected to begin, and therefore, this mechanism may be discounted.

For the microstructural condition which undergoes viscous glide controlled creep ($n = 3$) at low stresses, the greater stress sensitivity at higher stresses may also represent dislocation breakaway from solute atmospheres [27,39], the critical breaking stress being given by

$$\sigma_b = \frac{W_m{}^2 c}{5b^3 kT} \quad (4)$$

where c is the solute atom concentration in the matrix, and W_m is the binding energy between solute atoms and dislocations. Putting in appropriate numbers for the various parameters ($W_m \approx 3 \times 10^{-20}$ J, $c \approx 0.01$), we find that at 373 K, $\sigma_b/G \approx 3 \times 10^{-4}$. Since punch stress $\approx 3.5\sigma$, we obtain for the normalized breakaway punch stress, $\sigma_{b,punch}/G \approx 1.1 \times 10^{-3}$. Although this is close to the observed start of the high stress region, breakaway is unlikely to be the operative mechanism in the high stress regime for two reasons. First, following breakaway, the stress exponent n is expected to settle at a value corresponding to climb-controlled creep (i.e. $n \sim 4$–5) [27]. However, in the present case, the stress sensitivity in the high stress regime is considerably larger ($n_{app} \sim 9$). Secondly, while breakaway is a viable high stress mechanism when creep is glide-controlled at low stresses ($n = 3$), it is not consistent with climb-controlled creep in the low stress regime. As noted in Fig. 4, the beginning of a high n_{app} region can be discerned even when $n \approx 4.4$ in the low stress regime at 423 K. Furthermore, high stress exponents on the order of 9–11 have been frequently noted at high stresses in a range of studies [10,11,13–15,20], even in the absence of an $n = 3$ (viscous glide) region at low stresses, necessitating a mechanism other than breakaway to be invoked to rationalize the high stress behavior of Sn–Ag solders.

In order to gain insight into the mechanism operative in the high stress regime ($n_{app} \sim 8.6$–9.2) in Fig. 4, the data from this region was plotted as $(VT/G)^{1/n}$ versus σ_p/G, with $n = 6$–9 in increments of 0.5. Of these, $n = 6.5$ gave the best fit for all three temperatures (323, 373, and 398 K). Fig. 6 shows a plot of $(VT/G)^{1/6.5}$ versus σ_p, revealing that at each temperature, there is a temperature-dependent threshold stress σ_{th}, below which creep does not occur. The presence of this threshold stress suggests that the Ag_3Sn particles present in the microstructure play a role in determining the creep response of the alloy at high stresses. These observations are nominally consistent with those of reference 15 on Sn–Ag, where a true stress exponent of $n = 7$ was observed in conjunction with the presence of a threshold stress. This kind of behavior is usually attributed to particle-limited climb, where creep is controlled by climb of dislocation segments over particles, with the particle–matrix interface exerting an attractive force on the dislocation segment, and the threshold stress representing the stress required to cause thermally activated detachment of the dislocation segment from the particle [33]. The detachment stress σ_{th} may be expressed as [35].

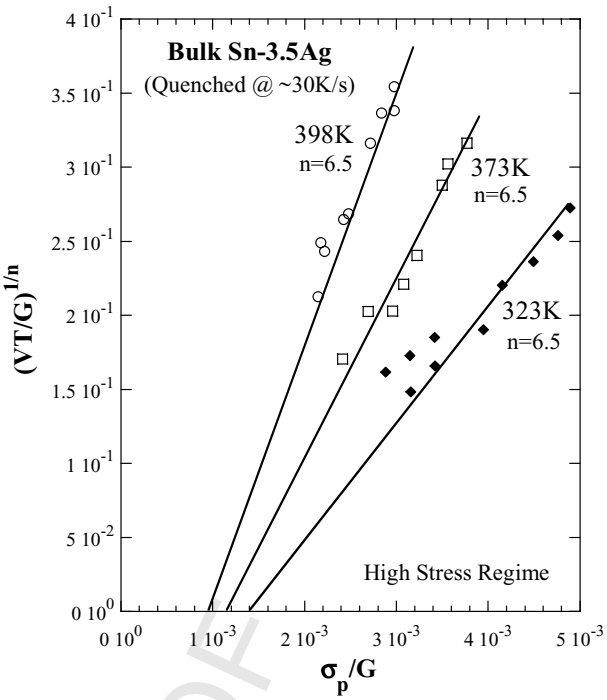

Fig. 6. Plot of $(VT/G)^{1/6.5}$ vs. σ_p, revealing that at each temperature, there is a threshold stress σ_{th}, below which creep does not occur. The threshold stress σ_{th} is weakly temperature dependent.

$$\sigma_{th} = \sigma_0\sqrt{1-k^2} \quad (5)$$

where $\sigma_0 \approx \sqrt{3}(Gb/\lambda)$ is the Orowan stress, λ the average interparticle spacing, and $k = \cos\gamma$ is a relaxation factor, γ being the equilibrium contact angle between the particle–matrix interface and the dislocation segment undergoing climb. For attractive particles, γ is between 0 and 90°. Image analysis of the as-reflowed microstructure shown in Fig. 1 has shown that the mean Ag_3Sn particle size in the divorced eutectic is 0.4–0.5 μm. Estimating the corresponding inter-particle spacing as $\lambda = 0.8$ μm, and assuming that $\gamma = 45°$, we obtain $\sigma_{th}/G \sim 4 \times 10^{-4}$, which is equivalent to a $\sigma_{p,th}/G$ (modulus compensated threshold punch stress) of $\sim 1.4 \times 10^{-3}$. This is very close to the values observed for $\sigma_{p,th}/G$ in Fig. 6 (1.4×10^{-3} at 323 K, 1.15×10^{-3} at 373 K, and 9.53×10^{-4} at 398 K). This strongly suggests that the particles indeed contribute to the threshold by the departure-site pinning mechanism proposed by Dutta [35]. Recalculating the data for the high stress regime by plotting $\ln(VT/G)$ versus $1/T$ for a constant value of $(\sigma-\sigma_{th})/G$, as shown in Fig. 7, we obtain for the true activation energy in this regime, a value of $Q \sim 61$–65 kJ/mole. These values are very close to the estimated value of 64 kJ/mole for dislocation core diffusion [15], which is clearly the operative diffusion mechanism. Furthermore, the n value of 6.5 is consistent with dislocation core diffusion controlled climb, the stress exponent for volume diffusion controlled climb being ~4.5, with the n increasing by an additional in-

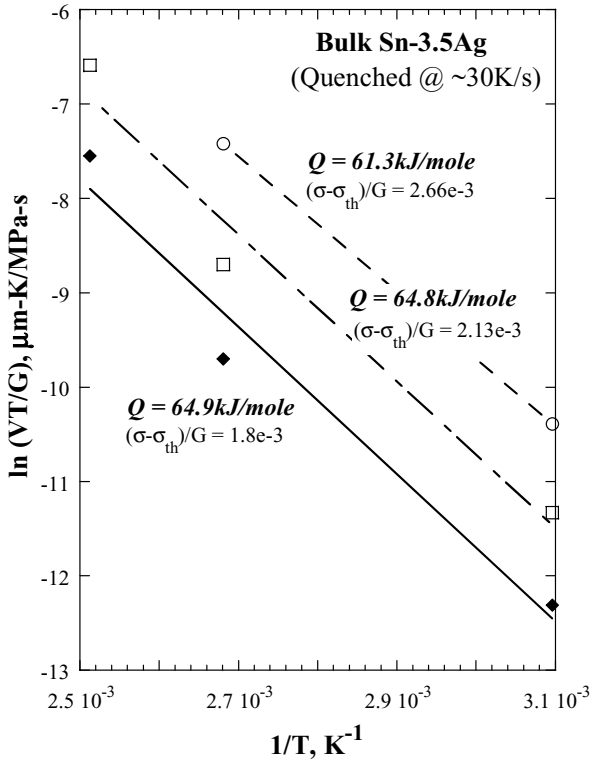

Fig. 7. Plot of $\ln(VT/G)$ vs. $1/T$ for a constant value of $(\sigma-\sigma_{th})/G$, showing that the true activation energy in the high stress regime, $Q \sim 61$–65 kJ/mole.

crement of two due to the stress-dependence of dislocation density.

As observed in Fig. 4, even at 423 K, where creep is climb-controlled in the low stress regime, the start of a transition to a high stress exponent regime at high stresses is discernible, although sufficient data are not available to conclude this with certainty.

4. Creep mechanisms in Sn–3.5Ag: a unified view

The present experimental results suggest that the creep response of Sn–Ag solders is controlled by the behavior of the divorced eutectic microconstituent which constitutes the continuous matrix in which the β-Sn dendrites are embedded, since it is the slower creeping of the two microstructural constituents. Based on the discussion in the preceding section, the total creep rate $\dot{\varepsilon}_T$ of Sn–3.5Ag solder may be written as the sum of two mechanisms, which occur simultaneously (i.e. in parallel with each other)

$$\dot{\varepsilon}_T = \dot{\varepsilon}_{gc} + \dot{\varepsilon}_{pc} \quad (6)$$

where $\dot{\varepsilon}_{gc}$ is the strain rate due to the glide-climb mechanism (where either viscous glide or climb is rate controlling), and $\dot{\varepsilon}_{pc}$ is the strain rate due to particle-limited climb.

As noted before, the glide-climb mechanism dominates the observed creep behavior at low stresses, whereas the particle-limited climb mechanism dominates at high stresses. A pictorial summary of these mechanisms is provided schematically in Fig. 8.

For the glide-climb mechanism, the rate controlling process is either viscous glide or climb of dislocations, which occur in series. The rate due to glide-climb can therefore be written as

$$\dot{\varepsilon}_{gc} = \frac{\dot{\varepsilon}_g \dot{\varepsilon}_c}{\dot{\varepsilon}_g + \dot{\varepsilon}_c} \quad (7)$$

where $\dot{\varepsilon}_g$ and $\dot{\varepsilon}_c$ are the rates of the viscous glide and climb processes, respectively. When $\dot{\varepsilon}_g \gg \dot{\varepsilon}_c$ (i.e. when the left side of Eq. (3) is much greater than the right side), $\dot{\varepsilon}_{gc} \approx \dot{\varepsilon}_g$, and this yields $n \sim 3$, as observed in Fig. 4 at 323–398 K. The corresponding creep rate is given by

$$\dot{\varepsilon}_g = A_g \left(\frac{Gb}{kT}\right)\left(\frac{\sigma}{G}\right)^3 e^{-Q_{Ag\,in\,Sn}/RT} \quad (8)$$

where the activation energy for diffusion of Ag in Sn, $Q_{AginSn} \approx 45$ kJ/mole.

If, on the other hand, $\dot{\varepsilon}_g \ll \dot{\varepsilon}_c$, the rate of glide-climb is given by $\dot{\varepsilon}_{gc} \approx \dot{\varepsilon}_c$, resulting in $n \sim 4.4$. Here, $\dot{\varepsilon}_c$ is given by

$$\dot{\varepsilon}_c = A_c \left(\frac{Gb}{kT}\right)\left(\frac{\sigma}{G}\right)^{4.4} e^{-Q_{Sn}/RT} \quad (9)$$

where Q_{Sn} is the activation energy for climb-controlled creep, and represents either volume or dislocation pipe diffusion in Sn. In the present work, Q_{Sn} was not determined, although an n value of 4.4 would typically suggest a volume diffusion-controlled climb mechanism, with $Q_{Sn} = Q_{vol} \approx 107$ kJ/mole. However, in Sn-based solders, an n value of 4–5 has also been associated with climb controlled by dislocation core diffusion, with $Q_{Sn} \sim 80$ kJ/mole [13]. Additional experiments are needed to determine Q_{Sn} for the highly refined microstructure of the present work.As noted in the previous section, the transition from climb-control to glide-control occurs below the σ_p/G range of the present data (Fig. 4), when a large, non-equilibrium amount of Ag is retained in solution in the β-Sn matrix in the eutectic region due to rapid cooling following reflow. This results in glide-controlled creep in the low stress regime. On the other hand, when, after extended exposure to elevated temperature (as for the sample tested at 423 K), the dissolved Ag concentration drops to near-equilibrium levels, the transition from climb to glide control can only occur at high σ_p/G values, allowing creep in the low stress regime to be controlled by climb. In either case, because of the presence of Ag_3Sn particles in the Sn-matrix (within the divorced eutectic region), a separate accommodation process must operate around the particles in order for the matrix to deform without causing decohesion at the particle–matrix interfaces. This can occur either by the generation of geometrically necessary dislocations around particles, or by stress-assisted diffusion along the particle–matrix interfaces, the latter being the likelier process at the low stresses of interest. Clearly, this accommodation process needs to occur more rapidly

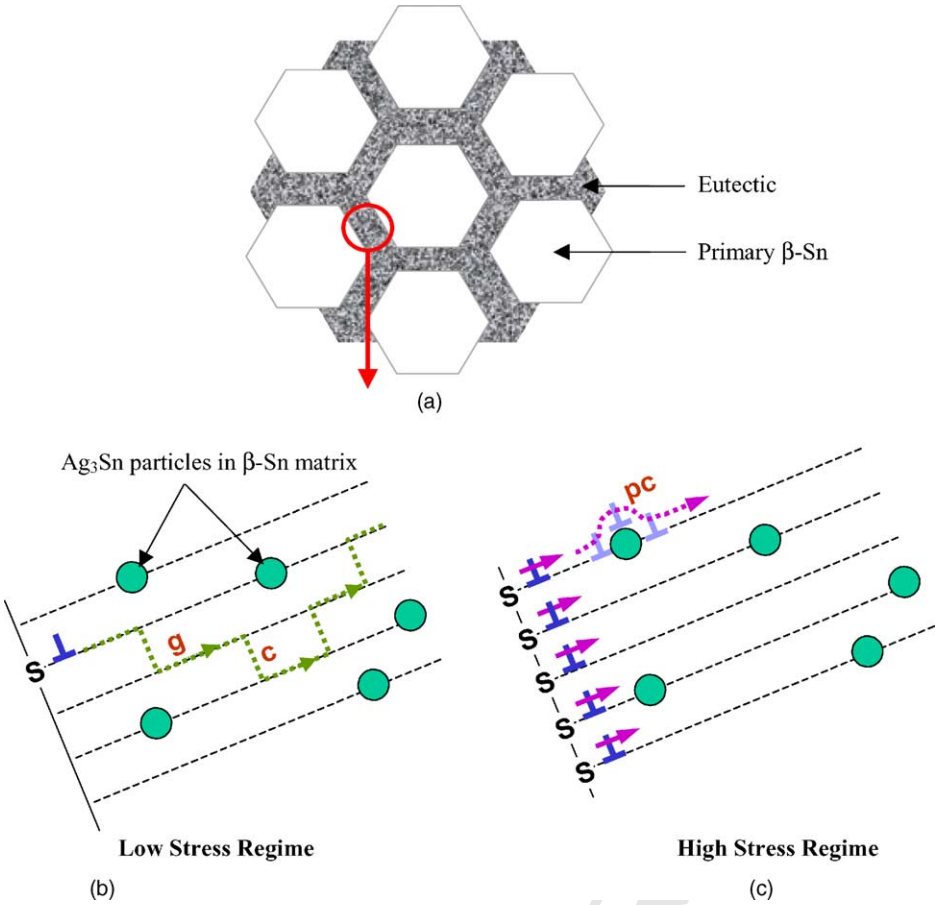

Fig. 8. A pictorial summary of the operative creep mechanisms in Sn–Ag. A schematic of the microstructure consisting of primary β embedded in a divorced eutectic matrix is shown in (a). The overall deformation of the "composite" microstructure is controlled by the behavior of the eutectic, which deforms via glide-climb ("g" and "c") at low stresses (b), and by particle-limited climb ("pc") at high stresses (c). Dislocation sources are represented by "S".

than the rate-controlling process. Indeed, at the high homologous temperatures involved, stress-assisted interfacial diffusion, which typically displays a low activation energy for many materials systems [36,37], is expected to be quite rapid.

In addition to dislocations that cause deformation by the glide-climb process by passing through the matrix regions between particles (~0.8–1 μm wide) as described above, many dislocations also get stuck at the Ag_3Sn particles. As σ_p/G increases, an increasing number of dislocation sources start operating (within the eutectic microconstituent, as well as at the primary β-Sn/eutectic boundaries), and the number of dislocations getting stuck at particles increases (see Fig. 8). Because of the attractive nature of the interfaces, these dislocations are unable to participate in deformation of the matrix via climb over particles at stresses lower than the detachment threshold. But once the Von–Mises equivalent stress exceeds the threshold stress for dislocation detachment from particle–matrix interfaces (σ_{th}), these previously stuck dislocations lead to a parallel deformation mechanism, particle-limited climb, with a strain rate of $\dot{\varepsilon}_{pc}$, given by

$$\dot{\varepsilon}_{pc} = A_{pc}\left(\frac{Gb}{kT}\right)\left(\frac{\sigma-\sigma_{th}}{G}\right)^{6.5} e^{-Q_{Sn,Pipe}/RT} \quad (10)$$

where $Q_{Sn,pipe} \approx 65$ kJ/mole is the activation energy for pipe diffusion in Sn, and the threshold stress sth is on the order of 3×10^{-4}G.[5] With increasing effective stress (*s*–sth), the rate of this mechanism increases rapidly, ultimately exceeding the rate of creep via glide-climb. In Fig. 4, this occurs at σ_p/G values around 1×10^{-3} to 3×10^{-3} at all temperatures. It should be noted that when tests are conducted only at high stresses, only the particle-limited climb mechanism is likely to be discernible, as in the recent work by Huang et al. [15], particularly when most of the excess solute has already precipitated out as Ag_3Sn particles. All data reported

[5] As seen in Fig. 6, the threshold stress appears to have a weak temperature-dependence, the modulus compensated threshold punch stress, $\sigma_{p,th}/G$, being 1.4×10^{-3}, 1.15×10^{-3} and 9.53×10^{-4} at 323, 378 and 398 K, respectively. This is equivalent σ_{th}/G values of 4×10^{-4}, 3.2×10^{-4}, and 2.72×10^{-4} at 323, 378 and 398 K, respectively.

in reference [15], as well as those re-analyzed in reference 15 based on previous work [40,41] correspond to $\sigma/G > 4.4 \times 10^{-4}$, which is equivalent to $\sigma_p/G > 1.5 \times 10^{-3}$, where, consistently with the present work, particle-limited climb operates. The presence of a high apparent stress-exponent ($n \sim 10.6$) region at modulus compensated shear stresses (τ/G) greater than $\sim 8 \times 10^{-4}$ (i.e. $\sigma_p/G \sim \sqrt{3} \times 3.5 \times 8 \times 10^{-4} \approx 5 \times 10^{-3}$), as noted in reference [13], is also nominally consistent with the transition from glide-climb control to particle-limited climb control noted in the present work at $\sigma_p/G \sim 2 \times 10^{-3}$–$3 \times 10^{-3}$).

Thus, in general, at low applied stresses, climb-controlled creep would be expected in Sn–3.5Ag for low levels of Ag supersaturation of the eutectic β-Sn, whereas a transition to viscous glide-controlled creep would be expected for high levels of supersaturation. At high stresses, the expected mechanism is core-diffusion controlled particle-limited climb with a threshold stress. The precise details of the operative creep mechanism(s), and the regime of transition from glide-climb to particle-limited climb, are of course, dependent on the solder microstructure, which in turn is strongly dependent on reflow (i.e. solidification) conditions [20,21].

5. Conclusions

The creep behavior of Sn–3.5Ag solder with a rapidly cooled microstructure was studied via impression creep testing. In the as-reflowed state, the microstructure, which consists of secondary dendrites of β-Sn interspersed with a highly refined divorced eutectic structure consisting of fine particles of Ag_3Sn in a β matrix, allows supersaturation of the β-Sn. At low stresses, this causes the solder to deform via viscous glide-controlled creep ($n \approx 3$) with the rate of glide being limited by diffusion of Ag through Sn ($Q \approx Q_{\text{AginSn}}$). At high stresses, where many more dislocation sources start operating, solder creep becomes controlled by dislocation interaction with Ag_3Sn particles (particle-limited climb), with the emergence of a threshold stress, $n \approx 6.5$, and an activation energy close to that of dislocation pipe diffusion in Sn ($Q \sim Q_{\text{Sn,pipe}}$). After limited aging of the microstructure which allows reduction of supersaturation, the $n = 3$ region is no longer observed, and is replaced by a dislocation-climb controlled regime ($n \approx 4.4$) at low stresses. The region of high stress sensitivity at high stresses, however, still appears to exist. Based on these observations, a unified view of the creep behavior of Sn–3.5Ag is presented. It is suggested that Sn–3.5Ag solders deform by two simultaneously operative, parallel mechanisms—glide-climb, which dominates at low stresses, and particle-limited climb, which dominates at high stresses, where dislocations climbing over attractive Ag_3Sn particles are able to detach themselves from the interface.

Uncited reference

[25].

Acknowledgements

The authors are grateful to Alpha Metals for supplying the solder used in this work gratis. This work is supported by an NSF-GOALI program in partnership with INTEL Corporation (grant #DMR-0209464) and SRC contract # 2002-NJ-1004. The collaboration and support of Drs. R. Mahajan, S. Jadhav and Fay Hua of INTEL are gratefully acknowledged. The authors thank Mr. Jesse Sherburn for his assistance with metallographic sample preparation. ID would also like to thank Prof. T.R. McNelley (NPS) for is guidance in interpreting the creep data, and Prof. K.L. Murty (NC State/NSF) for alerting him to the possibility of breakaway following viscous glide.

References

[1] V. Sarihan, Trans. ASME 115 (1993) 16–21.
[2] S.N.G. Chu, J.C.M. Li, J. Mater. Sci. 12 (1977) 2200–2208.
[3] E.C. Yu, J.C.M. Li, Phil. Mag. 34 (1977) 811.
[4] F. Yang, J.C.M. Li, J. Appl. Phys. 74 (1993) 4390–4397.
[5] D. Chiang, J.C.M. Li, J. Mater. Res. 9 (1994) 903–908.
[6] F. Yang, J.C.M. Li, Mater. Sci. Eng. A201 (1995) 40–49.
[7] D. Dorner, K. Roller, B. Skotzki, B. Stockhert, G. Eggeler, Mater. Sci. Eng. A, 2003, in press.
[8] H. Yang, P. Deane, P. Magill, K. Linga Murty, Proc. ECTC, 1996, pp. 1136–1142.
[9] R. Darveaux, K. Banerji, IEEE Trans. Comp. Hyb. Manuf. Technol. 15 (1992) 1013–1024.
[10] W. Yang, L.E. Felton, R.W. Messler, J. Electron. Mater. 24 (1995) 1465–1472.
[11] K.L. Murty, H. Yang, P. Deane, P. Magill, Proc. Interpak'97: Adv. Electron. Packaging ASME 19-1 (1997) 1221–1331.
[12] M.D. Mathew, S. Movva, H. Yang, K.L. Murty, Creep of Sn–3.5Ag and Sn–5Sb solders for electronic packaging, in: R.S. Mishra, A.K. Mukherjee, K.L. Murty (Eds.), Creep Behavior of Advanced Materials, TMS, 1999, pp. 51–59.
[13] H.G. Song, J.W. Morris, F. Hua, Mater. Trans. 43 (2002) 184–185.
[14] K. Wu, N. Wade, J. Cui, K. Miyahara, J. Electron. Mater. 32 (2003) 5–8.
[15] M.L. Huang, L. Wang, C.M.L. Wu, J. Mater. Res. 17 (2002) 2897–2903.
[16] E.A. Brandes, G.B. Brook (Eds.), Smithell's Metals Reference Book, Butterworth-Heinemann, seventh edition, 1992.
[17] P. Adeva, G. Caruana, O.A. Ruano, M. Torralba, Mater. Sci. Eng. A A194 (1995) 17–23.
[18] T. Reinikainen, J. Kivilahti, Metall. Mater. Trans. 30A (1999) 123–132.
[19] V.I. Igoshev, J.I. Kleiman, J. Electron. Mater. 29 (2000) 244–250.
[20] F. Ochoa, J.J. Williams, N. Chawla, The effects of cooling rate on microstructure and mechanical behavior of Sn–3.5Ag Solder, JOM, June 2003, pp. 56–60.
[21] P.T. Vianco, J.A. Rejent, J.J. Martin, The Compression Stress–Strain Behavior of Sn–Ag–Cu Solder, JOM, June 2003, pp. 50–55.
[22] F. Yang, J.C.M. Li, C.W. Shih, Mater. Sci. Eng. A201 (1995) 50–57.
[23] D. Pan, I. Dutta, A Complication of Impression Creep Tests and its Solution: Application to Sn–3.5Ag Solders, Mater. Sci. Eng. A, in press.
[24] S.N.G. Chu, J.C.M. Li, Mater. Sci. Eng. 39 (1979) 1–10.
[25] P. Adeva, G. Caruana, O.A. Ruano, M. Torralba, Mater. Sci. Eng. A194 (1995) 17–23.
[26] F.A. Mohamed, T.G. Langdon, Acta Metall. 22 (1974) 779–788.

[27] P. Yavari, T.G. Langdon, Acta Metall. 30 (1982) 2181–2196.
[28] C. Kittel, Introduction to Solid State Physics, fifth ed., Wiley, 1976, p. 100.
[29] R. Fiedler, A.R. Lang, J. Mater. Sci. 7 (1972) 531–542.
[30] T. Bieler, Michigan State Univerisity, Private Communication.
[31] F.A. Schmidt, J.C. Warner, J. Less Common Metals 26 (1972) 325.
[32] T.B. Massalski, (Ed.), Binary Alloy Phase Diagrams, second ed., ASM International, 1990, pp. 94–97.
[33] E. Arzt, J. Rosler, Acta Metall. 36 (1988) 1053–1060.
[34] Ansell, Weertman, Trans. TMS-AIME 215 (1959) p. 838.
[35] I. Dutta, J. Electron. Mater. 32 (2003) 201–207.
[36] J.V. Funn, I. Dutta, Acta Mater. 47 (1999) 149–164.
[37] K.A. Peterson, I. Dutta, M.W. Chen, Acta Mater. 51 (2003) 2831.
[38] O.D. Sherby, P.M. Burke, Prog. Mater. Sci. 13 (1967) 325.
[39] K.L. Murty, Scripta Met. 7 (1973) 899–904.
[40] H. Mavoori, J. Chin, S. Vayman, B. Moran, L. Keer, M. Fine, J. Electron. Mater. 26 (1997) 783–790.
[41] W.J. Plumbridge, C.R. Gagg, S. Peters, J. Electron. Mater. 30 (2001) 1178–1183.